JOURNAL OF GEOPHYSICAL RESEARCH, VOL. 103, NO. B5, PAGES 9879–9894, MAY 10, 1998

Quantifying the interaction of an ocean bottom seismometer with the seabed

John C. Osler[1] and David M. F. Chapman
Defence Research Establishment Atlantic, Dartmouth, Nova Scotia, Canada

Abstract. A theory is presented for the coupling between an ocean bottom seismometer (OBS), the sediments upon which it rests, and the surrounding water. Assuming that rotational and tilt effects are negligible (or have been made negligible through instrument design), the response of the OBS to forced harmonic motion is considered in both horizontal and vertical directions. Under these conditions it is concluded that the measured ratio of velocities when the OBS is on the seabed and when it is freely suspended in water (for an identical force) comp[illegible] characterizes the OBS/seabed interaction. This enables the velocity transfer functions to be directly calculated without recourse to a detailed model of sediment/structure interaction. An OBS was designed and constructed with good coupling to seabed motion and reduction of rocking effects as principal design criteria, including an onboard shaker to conduct in situ coupling experiments. The amplitude and phase of coupling data collected on a clay seabed provide transfer functions due to horizontal and vertical seabed motion and horizontal water motion. In addition, a simple mass-spring-dashpot model of OBS/seabed interaction permits the analysis of amplitude-only coupling data. Good vertical coupling can be achieved over a wide bandwidth by designing the sensor package to have a large hydrodynamic added mass in the vertical. Good coupling to horizontal seabed motion is more difficult to achieve but is possible within a limited bandwidth, even on very soft seabeds. Finally, an example of seismoacoustic noise is presented. Hydrophone signals are compared with horizontal geophone signals received from sources within the ocean and within the seabed, and the differences are explained in terms of the coupling transfer functions.

1. Introduction

Ocean bottom seismometers (OBSs) are used to measure the vertical and horizontal particle velocity of the seabed in ambient noise, earthquake, microseismicity, and controlled source seismic experiments. The ideal case of an OBS measuring the true motion of the seabed is difficult, if not impossible, to realize. The relative motion between an OBS and the surrounding seabed has been dubbed "coupling." Poor coupling manifests itself as resonances in measured signals [e.g., *Lewis and McClain*, 1977], elevated noise levels [e.g., *Latham and Nowroozi*, 1968], and distorted vector particle motions due to amplitude and phase corruption. The relative motion may be minimized by careful attention to instrument design [*Sutton and Duennebier*, 1987; *Duennebier and Sutton*, 1995] but cannot be entirely avoided due to the compliant nature of the seabed and the typical requirement that an OBS remain on the water/seabed interface to facilitate deployment and recovery. For vertical motion the seabed and water are constrained to move together, and a suitably designed OBS should exhibit little signal distortion. In the horizontal direction a discontinuity can exist between water and seabed particle motions, and good coupling is difficult to obtain, especially on soft bottoms.

The effects of OBS/seabed coupling were brought to the fore following the 1978 Lopez Island OBS Intercomparison Experiment. Colocated instruments were found to differ substantively in their response to the same forcing by transients and explosive sources and were significantly different than geophones fixed to the plate and spike standards. This experimental work was featured in a special issue of *Marine Geophysical Researches* [e.g., *Sutton et al.*, 1981a]. It also contained the original theories of vertical OBS coupling as proposed by *Sutton et al.*, [1981b] and *Zelikovitz and Prothero* [1981] based on a mass-spring-dashpot model and applied to Lopez Island data. Research into the OBS/seabed coupling problem has continued since this time. *Trehu* [1985] examined several detailed models of soil/structure interaction, concluding that simple frequency-independent compliance and damping parameters were adequate for most purposes. *Sauter* [1987] performed in situ calibrations of an OBS on various seafloors by comparing responses to forced motion with that obtained from a standard solid foundation on land. *Sutton and Duennebier* [1987] elaborated their theory for vertical OBS coupling to suggest several OBS design criteria, which were considered when designing the OBS used for the experiments in this paper [*Dodds et al.*, 1994; *Dodds*, 1994]. *Trehu and Sutton* [1994] demonstrated that auxiliary instrumentation deployed on the seabed in proximity to the OBS sensor package may influence the response function. *Duennebier and Sutton* [1995] present a theory for vertical and horizontal coupling which considers both translational and rotational motion. They conclude that the effects of rotational motion are inescapable for horizontal sensors and that they must be buried for high-fidelity measurements. In this paper we note an important unstated assumption in their formulation (which may be appropriate for the Office of Naval Research (ONR) instrument but may not apply to

[1]Now at SACLANT Undersea Research Centre, La Spezia, Italy.

Published in 1998 by the American Geophysical Union
Paper number 98JB00392.

102-03361/

other designs) and argue that (1) for some instruments the effects of rotational motion may be overestimated by their model; and (2) by quantifying the coupling transfer functions it is possible to determine a low-pass frequency band in which horizontal geophones on the seabed yield high-fidelity measurements. On soft sediments, the corner frequency of this low passband can be quite low; however, this is governed primarily by the translational dynamics and rocking effects can be made a secondary issue. (As we cite *Duennebier and Sutton* [1995] frequently, we will hereinafter refer to this reference as DS.) The signal distortion introduced by poor coupling, especially to horizontal seabed motion, is a principal concern in OBS measurements of absolute ambient noise spectra [e.g., *Kibblewhite and Ewans*, 1985], comparisons of OBSs and seismometers placed in boreholes [e.g., *Hedlin and Orcutt*, 1989; *Stephen et al.*, 1994], and in studies which require perfect instrument fidelity, such as full waveform inversions to determine shear wave attenuation [*Bibee and Dorman*, 1995]. For the many researchers who use travel time information from OBS measurements, poor coupling can be responsible for obscuring secondary arrival information (ringy data) and must be recalled by those who compare field records with synthetic seismograms. All of the aforementioned OBS measurements either require or would benefit from transfer functions for the coupling to seabed motion which are quantified in situ upon each deployment. At a minimum these transfer functions reveal the frequency band over which the instrument is well coupled and high fidelity is expected. Ideally, seismograms which are routinely corrected for "instrument response," which is typically the frequency response of the geophone and its associated preamplifier and gain stages, would also include corrections for the coupling response. However, this requires that the specifics of the seismoacoustic forcing be known, and this is not typically the case.

Our analysis of the coupling between an OBS and the sediments and water at the seabed follows the efforts of previous workers. We start with the equations of motion for the vertical [*Sutton et al.*, 1981b; *Zelikovitz and Prothero*, 1981] and horizontal (DS) cases, with the simplifying assumption that we may consider translational motion only. This assumption, which applies to OBS designs with sufficiently low height-to-base ratios, is justified in the appendix. Our innovation to the theory is showing that the in situ response of the OBS to forced oscillation can be inverted directly to provide the transfer function between seabed (or water) motion and OBS motion by taking advantage of the reciprocity in the equations of motion [*Trehu and Sutton*, 1994]. A particularly significant result is that the transfer functions are calculated without recourse to approximate expressions for sediment stiffness and radiation damping. The methodology also allows for the direct determination of several parameters (such as added mass quantities, spring coefficients, and damping coefficients) where others (DS) have had to rely on theoretical estimates. The theory has been applied in experiments with the Defence Research Establishment Atlantic (DREA) OBS, which conducts a coupling calibration in situ upon each deployment by forcing motion of the OBS with an internal shaker.

2. Theory: Coupling of an OBS to Motion at the Seabed

We first consider the response of an OBS to an oscillating force while freely suspended in water (i.e., the resonance frequency of the suspension is very much less than the drive frequency). We then consider the response of the instrument to an identical force while bottomed on the seabed. In effect, this comparison tells us all we need to know about the OBS/seabed interaction (provided both amplitude and phase are measured). We call the ratio of bottomed velocity to suspended velocity the coupling ratio. In practice, the suspended measurement only needs to be done once, and this can be done under laboratory conditions.

Next, we consider the response of the OBS to motion of the seabed or the water. We call the ratio of OBS velocity to seabed (or water) velocity the transfer function. The expressions for the coupling ratio and the transfer function both contain the seabed reaction, but this effect can be eliminated from the equation pair so that one can be expressed directly in terms of the other, without reference to the detailed physics of the interaction. Of course, one can always introduce a parameterized model of the OBS/seabed interaction if one wishes. In particular, coupling ratio data may be interpreted by applying a simple mass-spring-dashpot model. In section 2.3 we will illustrate the consequences of such a model. (In section 4 we apply both methods to a real data set.)

In what follows, all variables (forces, velocities, etc.) are assumed to be harmonic with angular frequency $\omega = 2\pi f$, although the time factor $\exp(j\omega t)$ is not written explicitly. Differentiation with respect to time becomes a multiplication by $j\omega$, so if v denotes velocity, then $j\omega v$ denotes acceleration and $v/j\omega$ denotes displacement. We will frequently refer to the OBS having a velocity "relative to the seabed," which should be interpreted to mean "relative to the velocity the seabed would have if the OBS were not present" or "relative to a seabed location removed from the OBS." We assume that the seabed material in direct contact with the OBS moves with it, so the motion of the OBS causes a local elastic deformation of the seabed from its natural motion.

We do not include rocking motion of the OBS and cross-coupling between horizontal and vertical directions, which we argue can be reduced to an issue of secondary importance. DS predict that horizontal geophone sensors in OBSs are subject to the effects of rotational motion and that there can be substantial cross-coupling of horizontal motion into vertical sensors. In the appendix, we note that DS have not included all contributions to the moment of inertia in their model. A computational model of OBS rocking motion needs to carefully consider the moment of inertia of the virtual mass of the water entrained in rotation of the coupling disk, which can be a significant term, as it scales as the radius of the coupling disk raised to the fifth power [*Lamb*, 1945; *Chung and Chen*, 1984]. For a suitably designed OBS, with carefully placed sensors and a coupling disk with a sufficiently large added moment of inertia and low center of mass, we argue that the effects of rotational motion are negligible. This assumption must be satisfied to permit the inversion we propose and is therefore given detailed consideration in the appendix. For other instruments, for which the moment of inertia and added moment of inertia are not sufficiently large, rocking effects can become considerable; in such cases, the more comprehensive model of DS would be required to model the OBS dynamics.

The theory presented here also does not include terms to account for the interaction with auxiliary instrument packages placed nearby on the seabed [*Trehu and Sutton*, 1994]. The DREA OBS consists of an acoustic sensor module (ASM) housing the geophones mounted on a coupling disk and a

surrounding frame which carries the auxiliary electronics and batteries. As with DS, when we speak of OBS motions and transfer functions, it should be understood that we are referring only to the motion of the ASM; however, we recognize the potential significance of interaction effects. We have extended the theory presented in this paper in a straightforward way to include the interacting motions of an auxiliary package, but the resulting expressions are only practical if the auxiliary package itself has motion sensors. (In effect, all modeled bodies must be OBSs.) As we have no calibration data for auxiliary bodies, we do not present the extended theory, although we discuss possible interaction effects in the particular case of the DREA OBS.

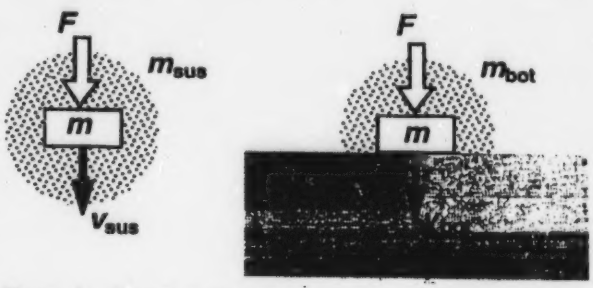

Figure 1. Forced motion of a suspended and bottomed OBS.

2.1. Response to Forced Oscillation: Coupling Ratio

Imagine an OBS of mass m freely suspended in water moving in response to a sinusoidal force F, as illustrated in Figure 1. The relation between this force and the resulting sinusoidal velocity v_{sus} follows from Newton's second law (mass times acceleration equals applied force):

$$j\omega(m + m_{sus})v_{sus} = F, \tag{1}$$

in which m_{sus} is the hydrodynamic added mass. This added mass is necessary to account for the reaction force caused by the acceleration of water which must move aside to permit passage of the OBS body [*Batchelor*, 1967]. (There is also a velocity-dependent drag force which is conventionally assumed to be too small to have a significant effect at seismic frequencies and amplitudes.) The mechanical impedance of the suspended OBS is F/v_{sus} or $j\omega(m + m_{sus})$.

If the oscillation were provided by a rotating shaft with an eccentric mass then the force would be

$$F = -\omega^2 a\,\delta m, \tag{2}$$

in which $a\,\delta m$ is the moment of the eccentric mass (ideally, a mass of δm at distance a from the shaft axis). With this applied force, v_{sus} would increase linearly with frequency, which is consistent with motion of a constant amplitude $a\,\delta m/(m + m_{sus})$; that is, the center of mass of the OBS would move so that the center of mass of the OBS plus eccentric mass remained stationary. (Although the theory presented below initially assumes an oscillating force, it is applicable to any reproducible forcing function analyzed in the frequency domain.)

Referring again to Figure 1, if we now bottom the OBS on the seabed, the seabed exerts a reaction force which we shall denote abstractly as the product of a frequency-dependent interaction impedance Z and the bottomed velocity v_{bot}. The total impedance of the bottomed OBS is $j\omega(m + m_{bot}) + Z$. We allow the bottomed added mass, denoted m_{bot}, to be different from m_{sus} to account for changes in flow patterns around the OBS when it is on the seabed and also for any added mass effects associated with the seabed sediments themselves. The Z term accounts for the seabed stiffness and damping. The equation of motion for the bottomed OBS is now

$$j\omega(m + m_{bot})v_{bot} = -Zv_{bot} + F. \tag{3}$$

The coupling ratio, i.e., the ratio between bottomed and suspended velocities for the same driving force, is

$$r = \frac{v_{bot}}{v_{sus}} = \frac{j\omega(m + m_{sus})}{j\omega(m + m_{bot}) + Z}. \tag{4}$$

Provided that Z/ω approaches zero as frequency increases, the high-frequency limit of the coupling ratio is simply a ratio of masses:

$$r_\infty = \frac{m + m_{sus}}{m + m_{bot}}. \tag{5}$$

Thus measurement of r_∞ provides m_{bot} if m and m_{sus} are known. (The appropriate limiting behavior of Z is assured by absorbing any mass-like linear-frequency terms into the added mass m_{bot}. For example, a simple spring-dashpot model behaves as required, having the form $Z = k/j\omega + R$, although we are not constrained to this simple model.)

So far, we have not distinguished between vertical and horizontal motion. Although the above expressions apply to both cases, the quantities m_{sus}, m_{bot}, Z, and r are, in general, different in these two directions.

2.2. Response to Seabed and Water Motion: Transfer Function

Now consider how the OBS moves in response to motion of the seabed below and the water above. We will treat horizontal motion of the seabed first, as it is conceptually easier.

2.2.1. Horizontal seabed motion. As illustrated in Figure 2a, if the seabed moves with horizontal velocity v_0 and the OBS responds by moving with horizontal velocity v while the water remains at rest, the OBS/seabed reaction force depends upon the relative velocity $v - v_0$, but the added-mass force depends only upon v, so the equation of motion of the OBS in the horizontal direction due to seabed forcing is

$$j\omega(m + m_{bot})v = -Z(v - v_0). \tag{6}$$

Solving for the ratio v/v_0, the transfer function for horizontal seabed motion is

$$T_h = \frac{v}{v_0} = \frac{Z}{j\omega(m + m_{bot}) + Z}. \tag{7}$$

To effect good transfer of horizontal seabed motion to the OBS, the mass and added mass in the horizontal direction should be kept as small as possible. Eliminating Z between (4) and (7), we find

$$T_h = 1 - r/r_\infty. \tag{8}$$

So, if the coupling ratio can be measured, the transfer function can be inferred, without recourse to a detailed physical model of the OBS/sediment interaction. The quantities T and r are generally complex, so both amplitude and phase of the coupling ratio need to be measured to directly determine the transfer function. Note that good coupling to horizontal sea-

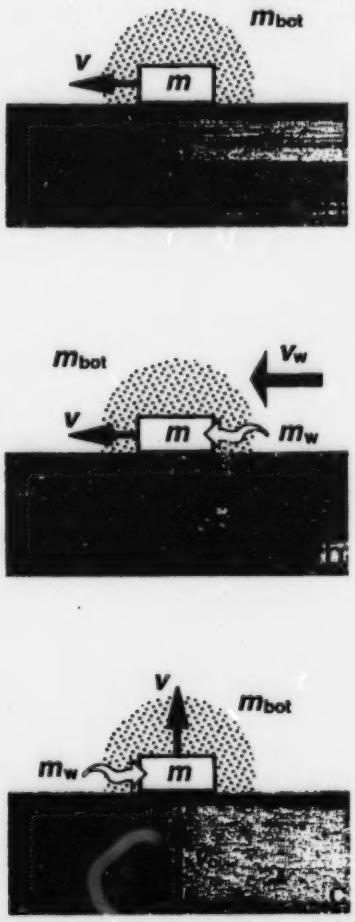

Figure 2. Response of bottomed OBS to (a) horizontal seabed motion, (b) horizontal water motion, and (c) vertical seabed motion.

bed motion requires that the coupling ratio r be much smaller than r_w. In other words, if the seabed resists forced motion of the OBS (relative to the freely suspended case), then independent motion of the seabed is faithfully transferred to the OBS. We will see that a simple mass-spring-dashpot model of OBS/seabed interaction defines an interaction resonance frequency below which there is good coupling to horizontal seabed motion.

2.2.2. Horizontal water motion without seabed motion. This case introduces a new force to the problem induced by water accelerating past the OBS. This force is equivalent to the force that would have been required to accelerate the water displaced by the OBS. This is described well by *Batchelor* [1967], but we prefer to analyze the dynamics of this case by transforming the problem to the accelerated frame of reference in which the water is instantaneously at rest.

Referring to Figure 2b, if the velocity of the OBS relative to the (stationary) seabed is v and the water velocity is v_w, then the OBS/water relative velocity is $v - v_w$. In the accelerated reference frame, there is an apparent horizontal gravitational field $-j\omega v_w$ giving rise to the apparent "net weight" $-j\omega(m - m_w)v_w$, in which m_w is the mass of water displaced by the OBS. (This apparent force is similar to feeling "heavier" in an elevator that suddenly begins to accelerate upward.) The equation of motion of the OBS in the horizontal direction due to water forcing is

$$j\omega(m + m_{bot})(v - v_w) = -Zv - j\omega(m - m_w)v_w. \quad (9)$$

Solving for the ratio v/v_w, the transfer function for horizontal water motion is

$$T_w = \frac{v}{v_w} = \frac{j\omega(m_w + m_{bot})}{j\omega(m + m_{bot}) + Z}. \quad (10)$$

To minimize the transfer of horizontal water motion, the displaced mass and added mass in the horizontal direction should be made as small as possible. Eliminating Z between (4) and (10), we find

$$T_w = \frac{r}{r_w}\left(\frac{m_w + m_{bot}}{m + m_{bot}}\right). \quad (11)$$

Measurement of the horizontal coupling ratio provides a direct indication of the transfer function between horizontal water motion and OBS motion. For a neutrally buoyant OBS ($m = m_w$), $T_w = r/r_w$.

2.2.3. Combined horizontal motion of the water and the seabed. This case is a straightforward combination of the two previous cases. If the seabed moves with velocity v_0 and the water with velocity v_w, the OBS/seabed relative velocity is $v - v_0$ and the OBS/water relative velocity is $v - v_w$, so the equation of motion of the OBS forced by horizontal motion of water and the seabed in the accelerated frame of reference is

$$j\omega(m + m_{bot})(v - v_w) = -Z(v - v_0) - j\omega(m - m_w)v_w. \quad (12)$$

As there are two independent driving forces, a simple transfer function cannot be defined. However, one can define the relation

$$T_{h+w} = v/v_0 = T_h + (v_w/v_0)T_w, \quad (13)$$

in which T_h and T_w are defined in (7) and (10), respectively. Thus one could possibly relate horizontal motion of the OBS motion to the true horizontal motion of the seabed if the ratio v_w/v_0 were known for the exciting seismic or acoustic wave. However, both the amplitude and phase of this ratio would be needed, and these quantities would vary with frequency, type of wave, horizontal wavenumber, etc. Accordingly, no universal calibration curve is possible for combined water and seabed motion in the horizontal direction.

2.2.4. Vertical seabed motion. In this case we again use the trick of transforming to the accelerated frame of reference in which the water is instantaneously at rest. As the seabed and the water are constrained to move together in the vertical direction, the seabed is also instantaneously at rest in the accelerated frame. Referring to Figure 2c, if the vertical motion of the seabed (and water) is v_0, then the OBS/seabed and OBS/water relative velocities are both $v - v_0$. In the accelerated frame of reference the apparent gravitational field $-j\omega v_0$ gives rise to the apparent "weight" $-j\omega(m - m_w)v_0$, so the equation of motion of the OBS in the vertical direction is

$$j\omega(m + m_{bot})(v - v_0) = -Z(v - v_0) - j\omega(m - m_w)v_0. \quad (14)$$

(Remember that m_{bot}, m_{sus}, Z, and r are generally different for vertical motion and horizontal motion.) Solving for the ratio v/v_0, the transfer function for vertical motion is

$$T_v = \frac{v}{v_0} = \frac{j\omega(m_w + m_{bot}) + Z}{j\omega(m + m_{bot}) + Z}. \quad (15)$$

Perfect coupling to the seabed motion is achieved for a neutrally buoyant OBS ($m = m_w$), regardless of the interaction impedance. This classic result has been derived without recourse to a detailed model of the OBS/seabed interaction. If neutral buoyancy is not possible (or not desirable), then it is advantageous for the OBS to have a very large added mass in the vertical direction, in contrast to the case of horizontal motion. Because the water is constrained to move with the seabed in this direction, coupling to the water motion is not a liability. Eliminating Z between (4) and (15), we find

$$T_v = 1 - \frac{r}{r_\infty}\left(\frac{m - m_w}{m + m_{bot}}\right). \quad (16)$$

In this case, good vertical transfer of motion can be achieved even if the coupling ratio is large, provided that the OBS is nearly neutrally buoyant and the vertical added mass is large.

2.3. A Simple Model of Interaction Between an OBS and the Seabed

We have derived some general properties of the interaction between an OBS and the seabed but have not yet introduced a specific model for the interaction impedance. If coupling ratio data are available for the OBS (obtained using an onboard shaker, for example), then the transfer function may be calculated directly. However, if such data are either not available or incomplete (perhaps the phase was not measured), then modeling the interaction may be necessary. In order to illustrate a realistic scenario we now assume a simple mass-spring-dashpot model of OBS/seabed interaction and examine the consequences.

The simplest realistic model of the interaction impedance is

$$Z = k/j\omega + R \quad (17)$$

in which k is a spring constant representing the reaction of the elastic seabed to displacement of the OBS and R is a damping constant representing loss of energy by radiation of interface waves or frictional dissipation. These constants are likely different for horizontal and vertical motion. Substituting this simple model in (4), the coupling ratio can be written

$$r = r_\infty \omega^2/(\omega^2 - \omega_0^2 - j\omega_0\omega/Q) \quad (18)$$

in which r_∞ has already been defined in (5), the resonance frequency ω_0 is

$$\omega_0 = \sqrt{k/(m + m_{bot})}, \quad (19)$$

and the resonance quality factor Q is

$$Q = \omega_0(m + m_{bot})/R = \sqrt{k(m + m_{bot})}/R. \quad (20)$$

Figure 3 illustrates the theoretical velocity response of an OBS to a rotating eccentric mass, whose force is given in (2), in the case of the simple mass-spring-dashpot interaction model. The suspended velocity shows a 20 log ω slope throughout, while the bottomed velocity shows a pronounced resonance. Above resonance, the bottomed response has the same slope (the OBS is moving with the water) but is 20 log r_∞ lower (assuming that the bottomed added mass is larger than the suspended added mass). At resonance, the bottomed response is 20 log Q higher than the suspended response. Below resonance, the bottomed response falls away steeply at a slope of 60 log ω. This is an idealized example but suggests the possibility of adjusting the parameters ω_0, r_∞, and Q (and hence k, R, and m_{bot}) to fit the mass-spring-dashpot model to measured coupling data. This model could then be used to calculate transfer functions. Alternatively, if no field data are available, one could estimate the quantities k, R, and m_{bot} and predict the coupling response for a given OBS design and seabed type.

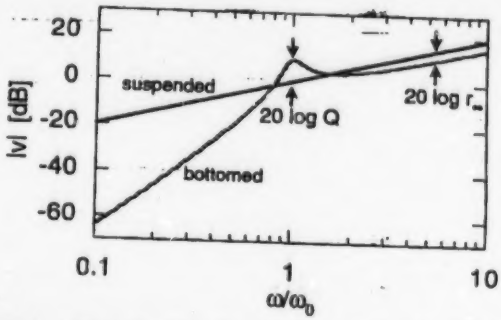

Figure 3. Expected velocity response of an OBS to forcing by a rotating eccentric mass.

The use of a frequency-independent spring constant may seem simplistic, especially when others such as DS use spring coefficients that are strongly frequency-dependent (to the extent of appearing to go negative). The resolution of this apparent discrepancy lies in a subtle difference between the two treatments. As *Trehu* [1985] explains, the base plate/seabed interaction is typically expressed as the sum of frequency-dependent stiffness (displacement) and damping (velocity) forces, which act in quadrature. (The coefficients could be regarded as the real and imaginary parts of a complex spring coefficient.) However, as acceleration is the second time derivative of displacement, an added-mass (acceleration) term is indistinguishable from a stiffness (displacement) term that is of opposite sign and proportional to the square of frequency (for harmonic motion). The DS spring coefficient functions are based on soil/structure interaction theory for dry-land structures, for which fluid added-mass terms are unnecessary and explicit sediment added-mass (acceleration) terms were apparently not considered. In effect, the sediment added-mass effect has been included in the spring coefficient and accounts for a substantial portion of the frequency dependence of that parameter. The two approaches, consistently applied, are effectively the same, but we prefer to explicitly identify the added-mass term as an independent parameter. This relieves our spring coefficient from the doing the work of an acceleration term, allowing it to have much weaker frequency dependence. (Furthermore, if the general frequency-dependent spring coefficient function is approximated by a second-order polynomial in frequency, a common approximation, this is mathematically identical to a model with a fixed spring constant and a fixed added mass. This approach eventually breaks down at frequencies well above resonance, but we are not so interested in modeling the response at these frequencies. *Trehu* [1985] has made similar observations.)

3. Experimental Procedure

3.1. OBS Design

The DREA OBS is designed to collect real-time calibrated measurements of ambient noise and controlled sources. The

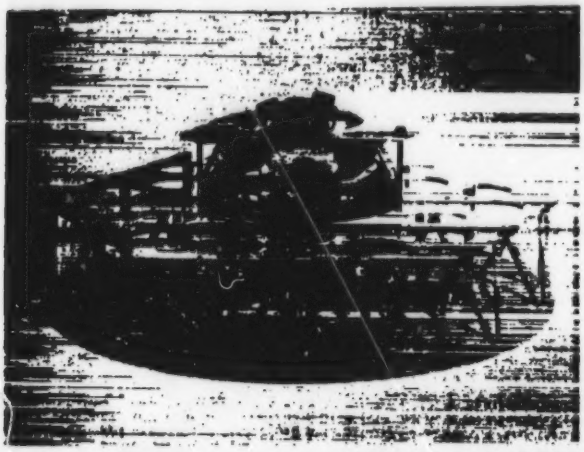

Figure 4. The acoustic sensor module (ASM) of the DREA OBS, showing the 0.25-m-diameter glass pressure vessel and the 0.66-m-diameter base plate.

acoustic sensor module (ASM), photographed in Figure 4, was built under contract according to DREA specifications. It consists of a hydrophone (DREA 31A96, 66 nF nominal capacitance) and an orthogonal triad of Mark Products L1-B geophones (resonance frequency 4.5 Hz, coil resistance 500 Ω). The geophones are all inclined at 54.7° to the vertical (the consequences of which are explained below) and mounted on a block which is leveled and clamped to the base of the 0.25-m-diameter spherical glass pressure vessel once the OBS has been deployed on the seabed. The pressure vessel is clamped to an aluminum coupling disk of radius 0.33 m. The coupling disk, seen in Figure 4, is formed by two concentric horizontal plates connected by a framework of rods based on a regular tetrahedral cell with a cradle for the 0.25 m spherical pressure vessel in the center. This design provides a coupling disk which is rigid below 50 Hz, while keeping its mass minimal.

The ASM includes several nonacoustic sensors (compass, temperature, pressure, and tilt) which are multiplexed on a slow data channel and can be continually monitored from the final stages of the instrument deployment until the early stages of recovery. Depth is measured with a PDCR910-1000 pressure transducer. Pitch and roll are measured with SSY0090 electrolytic tilt sensors. Temperature is measured with a National LM35CZ sensor. The KVH C-100 fluxgate compass is mounted in a small aluminum pressure vessel attached to the deployment frame. Tests have shown that an accuracy of a few degrees can be obtained if the compass is about 0.8 m away from the magnetic field of the geophones. As the ASM is not rigidly connected to the deployment frame, there can also be some rotation between the compass and ASM headings, but it is usually less than 10°. Typically, the orientation of the geophones is verified experimentally by determining the bearings at which there are nulls in their responses. Several continuous wave (CW) signals are projected while the research vessel proceeds along a circular track (typically of 3.7 km radius) which is centered on the OBS position.

The hydrophone and geophone outputs are digitized by Crystal CS5322/5323 24-bit delta-sigma analog-to-digital converters giving a dynamic range of more than 120 dB. When connected to a preamplifier based on the Linear Technology LT1012 operational amplifier, the self noise floor, including thermal and electrical contributions, is 20 dB below typical ambient noise levels [*Dodds*, 1994]. The signals pass through a second gain stage, remotely selectable in three 20-dB increments. The low self noise floor and large dynamic range allow the instrument to be used in a variety of experiments ranging from the collection of ambient noise in quiet environments to interface wave studies using explosive charges [*Osler and Chapman*, 1996]. As the mechanical design is of particular interest in coupling related studies, no further details concerning the electrical design will be included in this paper. Interested readers are directed to *Dodds et al.* [1994] and *Dodds* [1994].

For optimal coupling, the ASM mass has been minimized (m in equations (7), (10), and (15)) and is close to neutral density ($m \sim m_w$ in equations (10) and (15)), though slightly negatively buoyant for operational requirements. The height-to-base ratio is low, providing a large added mass in the vertical (m_{box} in equation (15)) and low added mass in the horizontal (m_{box} in equations (7) and (10)). The measured and estimated mass values are shown in Table 1. The radius of the coupling disk (0.33 m) is less than one quarter of a shear wavelength of the slowest speed materials likely to be encountered (e.g., clay seabed with shear speed of ~10 m/s and interface waves at 1–4 Hz [*Osler and Chapman*, 1996]).

To minimize the mass in contact with the seabed and possible interaction effects [*Trehu and Sutton*, 1994], the ASM is not rigidly connected to the surrounding deployment frame. The cords which connect the two are designed to slacken when the OBS is on the seabed, though they are not long enough to allow the ASM to touch the deployment frame. The deploy-

Table 1. Masses and Moments of Inertia for the DREA and ONR OBS Sensor Packages

	Formulation	ONR	DREA
Radius of sphere, m	r_i	0.17	0.127
Radius of disk, m	r_d	0.25	0.330
Density of water, kg m^{-3}	ρ_w	1003	1003
Mass of water displaced by instrument, kg	m_w	20.58	13.4
Inertial mass of sensor sphere, kg	m_i	38	8
Inertial mass of coupling disk, kg	m_d	negligible?	12
Virtual mass of water entrained in vertical motion of the OBS suspended in water, kg	$m_{sus} = \frac{2}{3}\rho_w r_d^3$	41.79	96.12
Virtual mass of water entrained in horizontal motion of the OBS suspended in water, kg	$m_{sus} = (2\pi/3)\rho_w r_i^3$	10.32	4.30
Moment of inertia of a sphere of uniform density about an axis passing through its center of gravity, kg m^2	$\frac{2}{5} m_i r_i^2$	0.44	0.05
Moment of inertia of coupling disk about a horizontal axis through its center, kg m^2	$m_d r_d^2/4$	negligible?	0.33
Added moment of inertia of the water entrained in rotation of the coupling disk (upper bound estimate), kg m^2	$\frac{16}{45}\rho_w r_d^5$	0.34	1.39

ment frame houses the deployment and recovery gear, power supply, and telemetry electronics; protects the ASM during deployment and recovery; and provides a terminus for the armored cable that carries the signals to the surface buoy. The deployment frame and ASM are initially positively buoyant, keeping the ASM off the seabed until the armored cable and surface buoy are decoupled from the ship. Upon command, the ballast tanks in the frame flood, the frame slowly sinks to the seabed, and the cords suspending the ASM slacken as the frame and ASM settle. Recovery is the exact reverse, air is pumped into the ballast tanks raising the frame and ASM off the seabed. The OBS deployment frame with suspended ASM is shown in Figure 5. The OBS frame is connected to a surface float by an armored cable with several hundred meters of cable left on the seabed to isolate the surface motion. A two-way digital telemetry link is maintained between the ship and the surface float. Incoming data are processed and displayed in real time. Outgoing commands control functions of the ASM such as leveling and clamping of the geophones, gain stages, frequency of the internal shaker during coupling calibrations, and ballast tank valves for deployment and recovery.

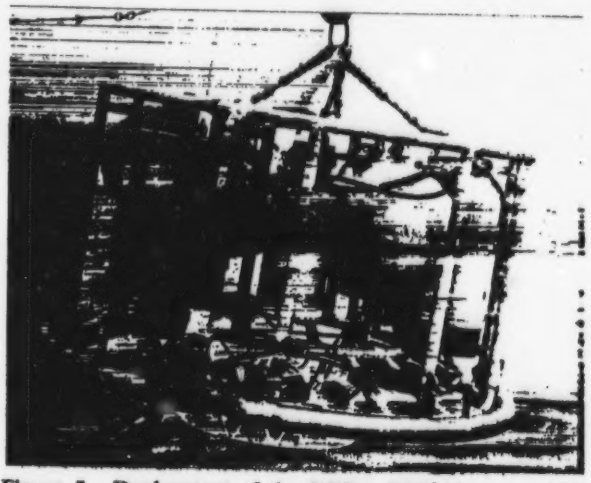

Figure 5. Deployment of the DREA OBS. Note the ASM suspended by ropes beneath the deployment frame.

3.2. Geophone Geometry and Component Resolution

As already described, the geophones are arranged such that they are orthogonal but all inclined equally to the vertical direction, resulting in a compact, symmetrical configuration. Assuming that any rotational motion is most likely to be about an axis through the center of instrument, this central, symmetric configuration for the geophones will reduce cross-coupling as the axes of the geophones intersect at the center of the base plate and rocking about this point results in motion perpendicular to the axis of all geophones. The raw data from the geophones in this configuration are a mixture of horizontal and vertical components, but these are easily resolved: the sum of the three geophone signals provides the vertical component, while the difference in signals between any pair of geophones gives a horizontal component. Three different horizontal components are resolved (H1, H2, and H3), each pointing in a direction 120° away from the others. Although this introduces redundancy, this can be regarded as an advantage, as a discrete source at any bearing will never be more than 30° off-axis in one of the horizontal channels, resulting in at most 1.25 dB reduction in signal level for that channel.

3.3. Coupling Data Collection and Reduction

Coupling experiments are conducted in situ upon each deployment by forcing the motion of the ASM at different frequencies in its 1–50 Hz operating band. The forcing is effected by a miniature DC motor mounted inside the pressure vessel driving an eccentric mass of ~1 g located ~0.5 cm off-axis. The motor axis is horizontal so that the excitation has both vertical and horizontal components. The phase of the forcing is tracked by a reflective infrared LED-phototransistor sensor which detects the passage of the eccentric mass through a reference point. The instrument is forced at each frequency for ~1 min. When multiple coupling experiments conducted during the same OBS deployment are compared, the ASM response is found to be stable and repeatable to within ±1 dB after an initial period of settling.

The time series data from the different channels are digitized at 125 Hz in the ASM and then spectrum-analyzed on the ship in real time or postprocessed in the laboratory. The length of each fast Fourier transform (FFT) is 512 points. Before applying the transform, the mean is removed from the samples and a Hanning window applied. There is a 50% overlap between points used in successive FFTs. Power spectral density estimates are calculated by averaging four FFTs. Calibrated signal levels, excluding the effects of the coupling transfer functions, are obtained by correcting the nominal signal levels for the sensitivity of the sensor, reference voltages, gain stages, nonunity frequency bin widths, and the Hanning window applied to the time series. (Note that our method for calculating coupling transfer functions does not require calibrated levels. The division of the response of the OBS when on the seabed by its response when freely suspended eliminates the effects of sensor sensitivity and any other system related transfer function.)

The DREA OBS has now been deployed at various locations on the Scotian Shelf, the passive continental margin of Nova Scotia, Canada (Figure 6). The surficial geology is dominated by the effects of the Wisconsinan Glaciation and relative sea level changes since glacial retreat. The prominent features are shallow banks (~100 m water depth) with sand as the surficial sediment type and deeper basins (150–300 m water depth) with clay and silt as the surficial sediment. On the Inner Shelf, there are outcrops of glacial till and the bedrock succession. For the purposes of this paper we have chosen data from a deployment at the clay site in Emerald Basin (Figure 6) as it demonstrates ASM behavior at, above, and below the resonance frequency of the coupling to a soft seabed.

The geoacoustic and oceanographic characteristics of the site in Emerald Basin (44°0.792'N, 63°1.308'W) are summarized by *Osler* [1994]. In brief, there is a wide diameter geotechnical core, side-scan sonar images [*Canadian Seabed Research, Ltd.*, 1996], and seismic reflection and refraction profiles using Huntec "boomer" [*Moran et al.*, 1991], air gun [*Louden*, 1994], and 3.5-kHz piezoelectric [*Canadian Seabed Research, Ltd.*, 1996] sources. The OBS was deployed in 219 m of water, over 9 m of LaHave Clay, and 29 m of Emerald Silt. The geotechnical core, 87003-002 [*Courtney and Mayer*, 1993], has a 17-m penetration with measurements of compressional wave speed, bulk density, water content, grain size, shear strength, impedance, magnetic susceptibility, and compressional wave attenuation at 500 kHz. The median grain size in the core is 2 μm,

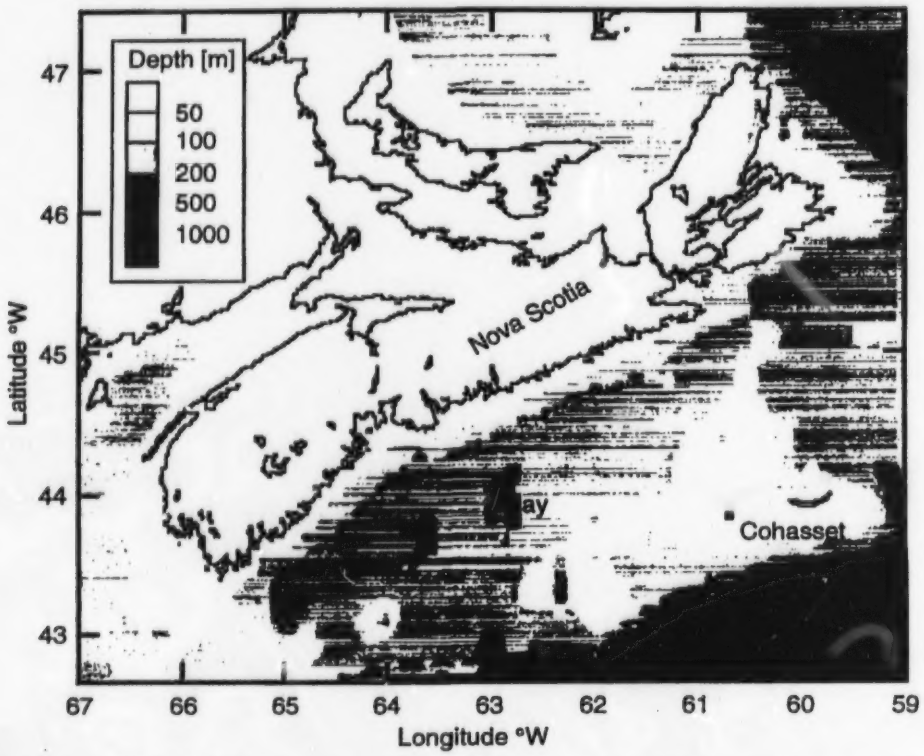

Figure 6. Map indicating the locations of the DREA OBS deployment on clay in Emerald Basin and drilling operations at the Cohasset oil field.

porosities range from 80% at the seabed to 55% at the base of the core, and bulk densities are ~1500 kg/m^3 for LaHave Clay and 1600 kg/m^3 for Emerald Silt. The compressional wave speed measured in the core is 1.45–1.49 km/s, consistent with field measurements of 1.46–1.49 km/s for LaHave Clay [*Dodds*, 1990]. The shear speed of the succession of clay and silt (determined by the dispersion of interface waves) ranges from ~10 m/s at the seabed to 120 m/s at 40 m depth [*Osler and Chapman*, 1996]. The shear speed profiles are consistent with a power law relationship of the form $c_s(z) = c_0 z^v$, with v in the range 0.60–0.65 and c_0 in the range 16–22 m/s referenced to (re) 1 m. Historical current meter observations from a mooring 30 km farther south in Emerald Basin [*Gregory and Smith*, 1988] reveal that the mean currents near the seabed are small, <0.01 m/s. Higher mean currents are observed at shallower depths (0.02 m/s at 50 to 100 m and 0.08 m/s at 20 m depth) but should not influence the ocean bottom deployment.

4. Results: In Situ Coupling Calibration

We propose two methods for inverting coupling ratio data to estimate the seabed/OBS velocity transfer functions. Method 1 requires both amplitude and phase of the coupling ratio data to be measured. Then the transfer functions can be calculated directly by substituting the measured coupling ratio data in (8), (11), and (16). (It must be emphasized, however, that no OBS/seabed interaction model is assumed or required.) Method 2 requires only the amplitude data to be measured, but the parameters of the mass-spring-dashpot model must be fit to the data using the amplitude factor of (18). Then the modeled transfer functions are calculated by substituting (18) into (8), (11), and (16) with the appropriate fitted parameters.

4.1. Method 1: Direct Calculation Using Amplitude and Phase of Coupling Data

Figure 7 shows the amplitude of the velocity of the OBS in response to forced vibration in both horizontal and vertical directions when freely suspended and when bottomed on a clay seabed, along with the bottomed-minus-suspended phase difference. The velocity units are decibels relative to 1 pm/s (10^{-12} m/s). The horizontal channel is H3, in the plane of the shaker motion. (A similar response is seen on horizontal channels H1 and H2 but with the amplitude reduced by 6 dB in accordance with the 60° angle between the forcing and the channel axes.) Above resonance, the bottomed amplitude data parallel the suspended data, and may be considered coincident within the scatter of the data; below resonance, the bottomed amplitude data fall off steeply. Note that the suspended data show a 20 log f slope, as expected. In effect, this measurement calibrates the force supplied by the shaker. The bottomed amplitude data exhibit the behavior expected from the simple mass-spring-dashpot model of OBS/seabed interaction illustrated in Figure 3.

The resonance frequencies for horizontal and vertical coupling are about 7.4 Hz and 9.8 Hz, respectively. Of course, one would like these resonance frequencies to be higher, but they are similar, if not slightly better, than other published results on a soft seabed. When the sensor package of the new ONR

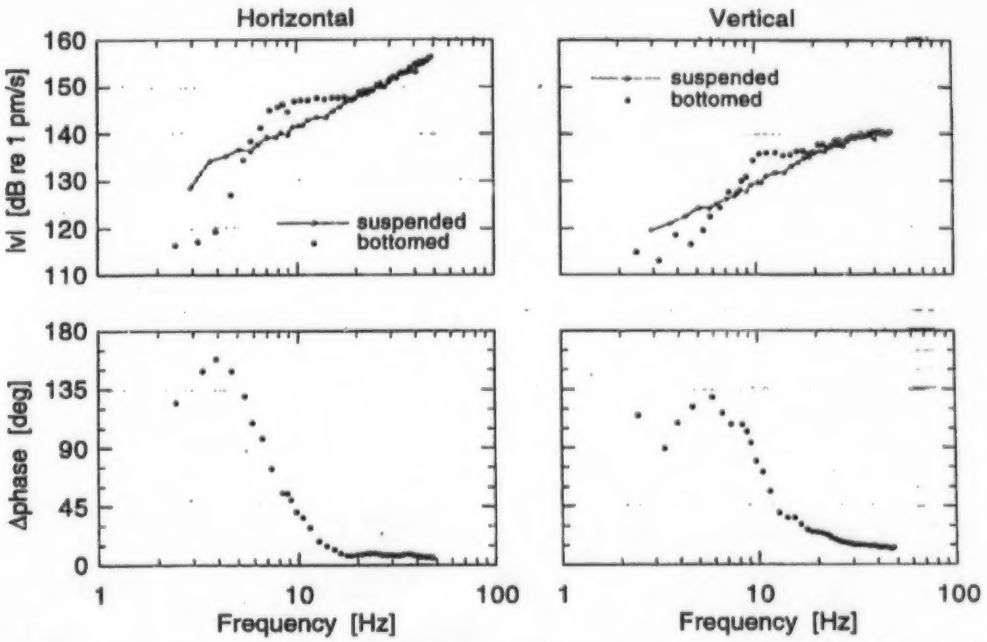

Figure 7. Amplitude and phase of OBS velocity in response to forced vibration. Solid symbols, bottomed on clay seabed; connected shaded symbols, suspended in water tank.

OBS was deployed on material with a shear wave speed of 12 m/s [*Trehu and Sutton*, 1994], resonance frequencies of 7–9 Hz were observed in response to vertical transients and 3 and 4 Hz in response to horizontal transients (with a secondary resonance at 7 Hz). Furthermore, the resonance frequency for vertical motion of the ONR OBS is consistent with the predictions of DS when a shear wave speed of 10 m/s is specified. In an effort to increase the resonance frequency on soft materials, DREA has conducted experiments with a set of three radial vanes (0.133 m in height) attached to be the base of the coupling disk [*Dodds*, 1995]. It was hoped that this increase in the inertial mass of the ASM (a total of 3.2 kg), and possibly virtual mass in the horizontal, would be offset by the benefits of coupling the instrument into stiffer sediment. Results from initial experiments with the OBS deployed with vanes at the same site (within 200 m) are not conclusive. The resonance frequency for horizontal motion increases marginally (1–2 Hz) and is more heavily damped. Unfortunately, a secondary resonance is introduced at 10.8 Hz, and it is particularly noticeable in the vertical channel.

The magnitude of the coupling ratio for each data set was calculated by subtracting the interpolated suspended velocity data from the corresponding bottomed velocity data. (Interpolation was necessary because the suspended and bottomed data were not measured at precisely the same frequencies.) The phase of the coupling ratio is the same as the bottomed-minus-suspended phase difference. In order to perform the direct calculation of the transfer functions T_h, T_w, and T_v using (8), (11), and (16), it was necessary to estimate the quantity r_∞ from the offset between suspended and bottomed data: we found that $r_\infty \sim 0.97$ in the horizontal and $r_\infty \sim 0.95$ in the vertical. (These values were actually determined from the curve fits in section 4.2, but the results would have been essentially the same had we simply assumed $r_\infty = 1$ in each case.) Using (5) and the mass quantities in Table 1, these r_∞ values correspond to bottomed added masses of $m_{bot} = 5.1$ kg in the horizontal and $m_{bot} = 102$ kg in the vertical.

The directly computed transfer functions for the clay deployment are shown in Figure 8, indicated by the discrete data points. The transfer function for vertical motion is within 0.75 dB of unity at all frequencies, by virtue of the large hydrodynamic added mass which the coupling disk provides. We regard this correction to be insignificant for most OBS applications and consider the vertical response of the ASM to be an accurate rendering of the true seabed motion in its 1–50 Hz operating band. This is not the case for the transfer functions for horizontal motion. Below resonance, the ASM is coupled to seabed motion with the amplitude and phase distortion progressively decreasing at lower frequencies. Above resonance, the ASM moves with the water and is not coupled to the motion of the seabed. At the resonance, the ASM responds to the combined motion of the water and the seabed: the response to seabed motion lags by 90°, whereas the response to water motion leads by 90°, resulting in a phase difference of 180° between the two responses. The phase responses show some scatter but only at very small phase values or when the magnitude response is very small, so the scatter is not significant. (Also in Figure 8 we have included the modeled transfer functions based on method 2, described in section 4.2.)

4.2. Method 2: Indirect Calculation Using Model Fit to Amplitude Only

The second method to calculate the transfer functions requires a model of OBS/seabed interaction to be fit to the coupling data. The method can be used with instruments which can measure the amplitude of the forced response (by external transient pulls or an onboard shaker) but do not have the ability to measure the phase. The coupling data may also be

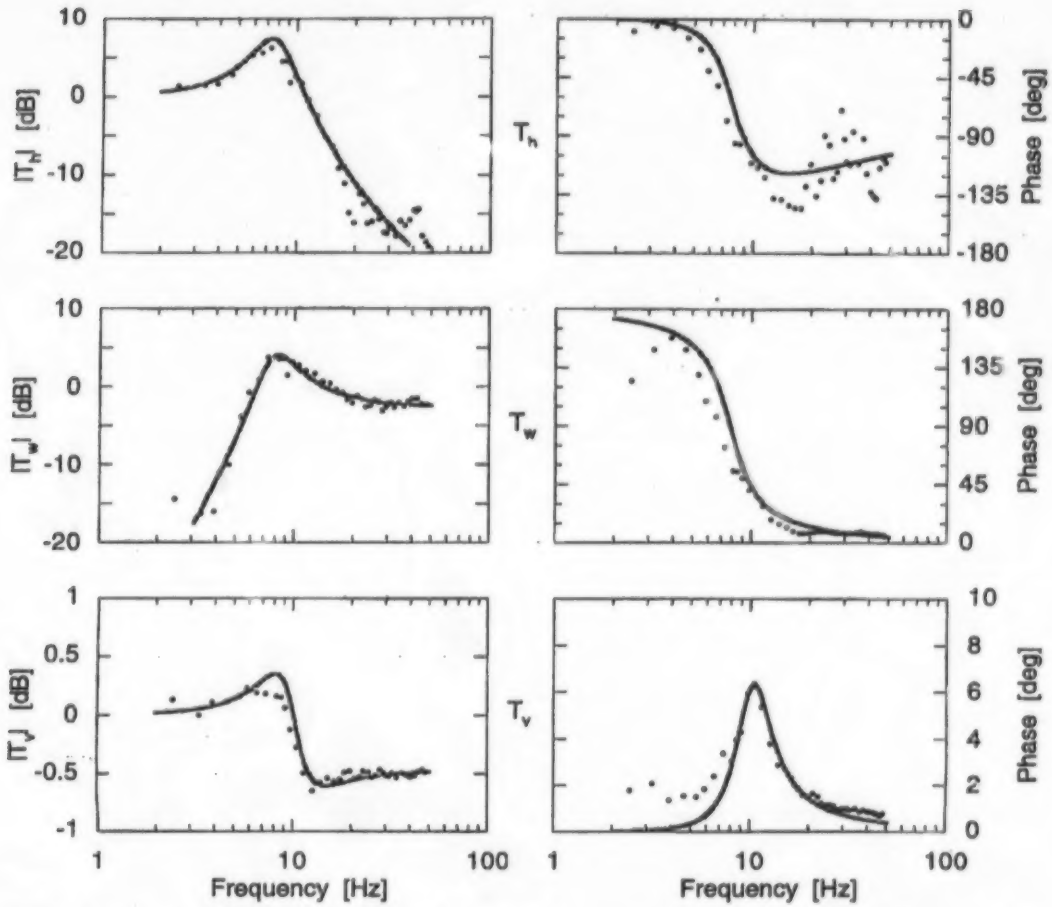

Figure 8. The seabed/OBS transfer function for the deployment on clay. Symbols, direct computation from amplitude and phase of coupling data; lines, computed from model fit to amplitude of coupling data. (Note change of scales for vertical transfer function.)

used to gain insight into the physical properties of the medium by comparing the predictions of diverse models for soil/structure interaction with the actual response, but that is not our objective in this paper.

In Figure 9 we plot the coupling ratio data (amplitude only), i.e., $|v_{box}/v_{sub}|$, for the clay seabed with both horizontal and vertical forcing, along with the model curve fits for each case. Equation (18) was fit to each data set by adjusting the parameters r_∞, f_0, and Q using the NonlinearFit algorithm in the Statistics package of Mathematica®, version 2.2.2. [*Wolfram*, 1991]. Because the data deviates from the model response at very low frequencies, data below the frequency f_{min} were not

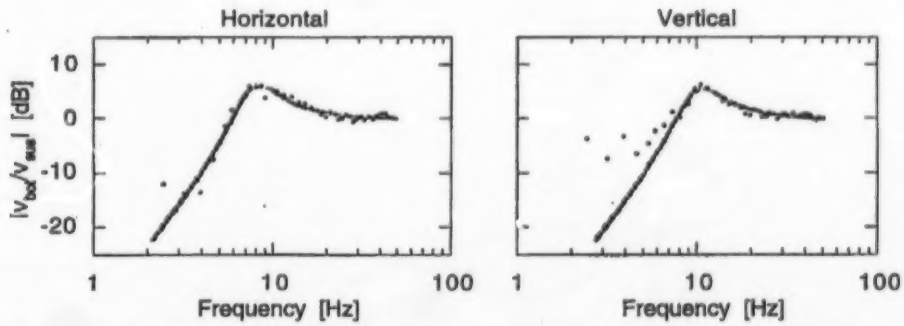

Figure 9. Fit of simple model of OBS/seabed interaction to coupling ratio data collected on a clay seabed. Solid circles, data used in model fit; open circles, data ignored in model fit; curves, method 2 model fit.

included in the curve fit. We offer two explanations for this behavior at low frequency. First, the mass-spring-dashpot model may not fully describe the physics of the OBS/seabed interaction below the obvious resonance. Second, this may be evidence of low-frequency interaction effects between the ASM and the deployment frame, an issue to be discussed below.

The parameters for the resulting fits are shown in Table 2, along with the values of f_{min} and the inferred values of m_{bot} for each case. (The mass m_{bot} was calculated from r_∞ and the masses from Table 1, using equation (5).) Using the curve-fit parameters from Table 2, the modeled complex coupling ratios were calculated from (18), including amplitude and phase factors. Then the modeled transfer functions were calculated by substituting (18) into (8), (11), and (16) with the appropriate fitted parameters. In Figure 8 the direct (method 1) and indirect (method 2) transfer function calculations are compared. The correspondence between the two methods is good and validates the applicability of the simple mass-spring-dashpot model of OBS/seabed interaction. However, it must be emphasized that the direct calculation of the transfer functions from the amplitude and phase of the coupling data does not require such a model, and consequently, it is a more general method.

4.3. Discussion of ASM/Frame Interaction Effects

The anomalous low-frequency coupling data in Figure 9 may be evidence of interaction effects between the ASM and the deployment frame, as considered by *Trehu and Sutton* [1994]. To investigate these effects, we devised a straightforward extension to the theory presented above. The simplest interaction model consists of two similar (although not identical) mass/spring systems, one representing the sensor package and the other representing the auxiliary package, independently driven by seabed forcing but also weakly coupled to one another by a third spring. Assuming that the resonance frequency of the auxiliary package is much lower than that of the sensor package and the coupling between the packages is weak, the response of the sensor package is essentially the same as the uncoupled case, with the exception of some mild structure at the auxiliary package resonance frequency. In the light of our coupling data for the DREA OBS on the clay seabed this suggests that the frame may have a resonance at very low frequencies, and there may be some frame/ASM interaction at this frequency. However, the modeling also suggests that the coupling data over almost all the bandwidth is suitable for calibration purposes using the non-interacting theory, as the ASM is effectively decoupled in that band.

Our deployment constraints demanded an auxiliary package, thus exposing the OBS to potential interaction effects, but we made efforts to mitigate these effects. ASM/frame interaction is a possible shortcoming of the current DREA instrument but does not detract from the main thrust of this paper, which is the theory of instrument/seabed coupling for an independent instrument. Consideration of interaction effects between the sensor package and auxiliary package of an OBS is a serious concern and deserves further investigation, both theoretical and experimental.

4.4. Example: Underwater Ambient Noise on a Geophone and a Hydrophone

Sonograms of ambient noise on the hydrophone and one of the horizontal geophone channels (H3) during an experiment at the clay site in Emerald Basin are shown in Figure 10. The calibrations applied to the spectra account for all factors (sensitivity, reference voltages, gain stages, analysis bin width, and windowing) except the coupling transfer functions. Each spectral frame is representative of a 30-s sample of data (the average of six 512-point FFTs with a 39% overlap between points in successive FFTs). The dynamic range of the sonograms is 70 dB, 55–125 dB re 1 μPa for the hydrophone and 51–121 dB re 1 pm/s for the geophone. (Our reference units are selected to account for most, 120 dB, of the approximate in-water conversion from pressure to velocity of 123.5 dB. For the line spectra, beneath the sonograms in Figure 10, the remaining offset is helpful in distinguishing the hydrophone and geophone curves, particularly at higher frequency.)

Table 2. Parameters for Curve Fits of Simple Model to Coupling Ratio Data

	r_∞	f_0, Hz	Q	m_{bot}, kg	f_{min}, Hz
Clay (horizontal)	0.97	7.8	2.1	5.2	3.4
Clay (vertical)	0.95	10.0	1.9	105	8.5

The loud noise band of 17–27 Hz on both sensors is caused by finback whales, *Balaenoptera physalus* [*Watkins et al.*, 1987]. The vocalizations from an individual whale are ~2-s-long swept frequency bursts which are repeated every 10 to 12 s. As can be seen in the sonograms, the bouts of vocal activity are separated by quiet periods of varying duration. The three narrowband lines at 6.4 Hz, 9.6 Hz, and 12.8 Hz (more prominent on the hydrophone) are the first, second, and third harmonics of a 3.2-Hz fundamental that is buried in the extremely-low-frequency noise ramp below 6 Hz. (Such harmonic sets, associated with diesel engines, in this case from CSS *Parizeau*, are frequently seen in ocean ambient noise spectra.) As the R/V *Parizeau* progressed away from the DREA OBS on a radial track, the intensity decreased with time (range) and a regular pattern of multipath interference was established (intensity peaks and valleys which are most easily seen on the 6.4-Hz line).

An additional very strong narrowband signal was sensed by the geophone but not observed on the hydrophone. The nominal frequency is 6 Hz, but it varies in an unpredictable manner (unlike doppler shifts from transiting vessels). The signal is intermittent but not in a systematic manner as expected for multipath interference. Last, the 6-Hz energy was also observed on the geophone sensors of colocated OBSs deployed by Dalhousie University [*Louden*, 1994]. These observations suggest that the energy comes from an independent source and that it is not an artifact of the instrumentation or its coupling to the seabed. Upon further investigation, it was determined that the 6-Hz energy was related to drilling operations at the Cohasset oil field (S. F. Kroetch, LASMO Nova Scotia Limited, personal communication, 1994) which is 190 km from the DREA clay site at a bearing of 100° true (Figure 6). Drilling logs for the day in question reveal that the drill bit was rotating between 320 and 370 RPM at a depth of ~1200 m below the seabed. The onboard compass and a circular projector tow were used to determine the orientation of horizontal geophone component H3 of the DREA OBS, bearings 81° true and 87° true, respectively. When spectra from the three geophone components are compared, the response at 6 Hz on H3 is consistently higher (by 2 dB or more) than on H1 and H2. Considering that there is no appreciable signal on the hydrophone at this frequency, it is likely that these are shear wave arrivals, probably steeply arriving *SV* waves. The strong signal

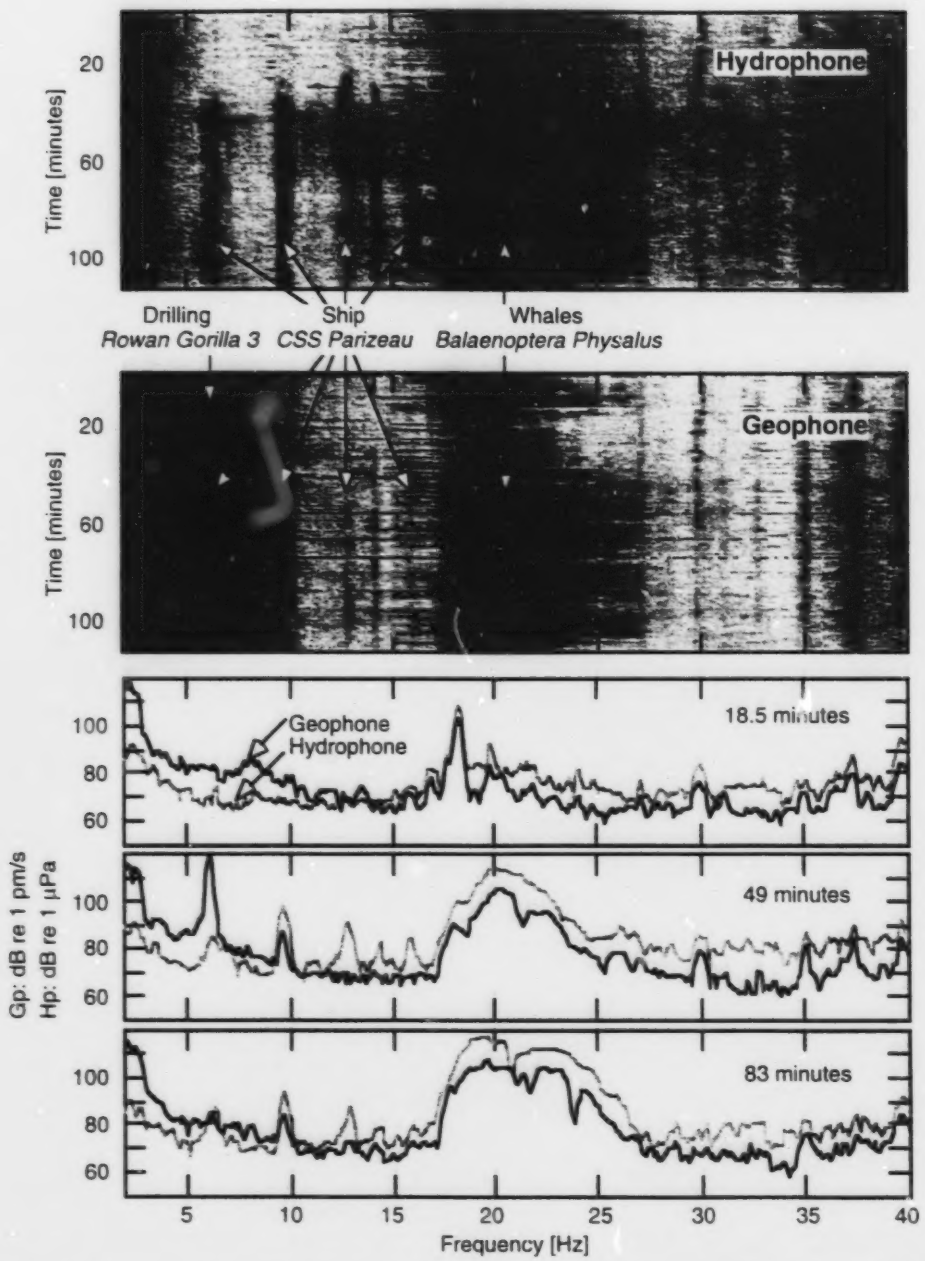

Figure 10. Sonograms of ambient noise on the hydrophone and the horizontal geophone channel H3 at the clay site and three comparisons of their spectra when different acoustic and seismic noise sources were active. The times refer to the temporal position of the spectral frames in the sonograms.

on H3 is thus consistent with the source being drilling operations at the Cohasset oil field. Why signals from a rotating drill would be preferentially generated and/or transmitted in the *SV* polarization rather than *SH* would make an interesting study.

Spectra from three different 30-s time intervals are also displayed in Figure 10. At 18.5 min, there are no whale vocalizations, no drilling activity, and no lines from R/V *Parizeau*, while at 49 min, all three sources are active. At 89 min, R/V *Parizeau* is farther away, and there is no drilling noise. In interpreting the ambient noise spectra it is of significance that the 6-Hz line is a seismic signal arriving at the OBS through the seabed with a negligible component in the water. The harmonic set, by contrast, is essentially an acoustic signal from a water-borne source and the geophone channel senses the second and third harmonics of the acoustic signal, but the first harmonic is washed out by the strong seismic line. The horizontal channel senses the drilling related noise at 6 Hz because it is primarily sensitive to seabed motion below the 7.8-Hz resonance frequency of the coupling (Figure 8). Above this resonance frequency, it is primarily sensitive to water motion,

and generally speaking, the hydrophone and geophone spectra exhibit the same characteristics at the higher frequencies (apart from the offset due to the units selected and some differences related to the directionality of the geophone sensor). The spectral characteristics begin to differ as the frequency decreases through the coupling resonance.

5. Conclusions

We have derived transfer functions for OBS coupling to vertical and horizontal motion of the seabed, horizontal motion of the water, and combined motion of the water and seabed. The novelty in our approach is formulating the transfer functions in terms of the ratio of instrument response to forced motion when it is bottomed on the seabed and when it is freely suspended in water. This approach provides a straightforward and elegant technique to quantify the OBS/seabed interaction. It does not require approximate expressions for sediment stiffness and radiation damping and allows the direct calculation of several parameters, such as hydrodynamic added mass terms. A further advantage of using the coupling ratio is that any system-dependent factors (gain stages, frequency response, filters, etc.) are removed when the responses are divided.

In principle, our technique may be applied to any OBS, provided that (1) the force applied when bottomed and when suspended is repeatable and (2) the instrument is insensitive to rotational motion. While our instrument uses an internal shaker to force motion, the theory is valid for any forcing, such as an impulse from a released weight as has been used in many coupling experiments. The direct calculation of the transfer functions (method 1 above) requires the difference in phase between the bottomed and suspended responses. If the phase cannot be measured, then the transfer functions may be calculated from the amplitude responses. This requires a model of the OBS/seabed interaction to be fit to the coupling ratio data (method 2 above). We have compared our transfer functions calculated using a simple mass-spring-dashpot model (fitting the three parameters r_∞, f_0, and Q) for the OBS/seabed interaction to the direct calculation and found them to be quite adequate.

An objective of this research was to obtain calibrated measurements of ambient noise, including the coupling transfer functions. However, most seismic or acoustic waves have components of motion which are both in the water and in the seabed requiring that a transfer function be calculated for each specific wave type, angle of incidence, and seabed type. Nonetheless, the coupling transfer functions indicate the bandwidth over which the instrument is coupled to seabed motion and the fidelity of the motion. Ambient noise collected with the DREA OBS is consistent with the calculated transfer functions. The instrument sensed seismic signals in the band in which it is coupled to seabed motion and had a similar response to a colocated hydrophone in the band in which the OBS is coupled to water motion.

Good coupling to vertical seabed motion is easily realized by providing a base plate with a large hydrodynamic added mass in the vertical. Achieving good coupling to horizontal seabed motion on soft bottoms, with a wide bandwidth and minimal amplitude distortion, is a difficult challenge when the instrument must rest on the water/seabed interface. However, it is possible for a sensor package resting on the seabed to provide high fidelity measurements to horizontal motion within a limited band, which is determined by design of the instrument and the rigidity of the seabed material.

Appendix: When Is Rocking Important?

The theory of OBS/seabed coupling proposed in this paper makes the simplifying assumption that rocking is unimportant, allowing the effective motion of the OBS to be described by decoupled linear translations in the horizontal and vertical directions, even when the forces do not all act through the center of mass (CM). This appendix justifies this assumption for a class of OBS instruments, such as the DREA OBS, that have been specifically designed to mitigate rocking motion. Although rocking effects cannot be entirely eliminated, they can be reduced to an issue of secondary importance through judicious design. For instruments for which rocking effects are significant, the full equations of motion of DS must be considered. Although the dynamical equations in the main text could be viewed as simplifications of the more comprehensive DS model, we have derived them in a straightforward way from first principles under the stated simplifying assumption. The following analysis introduces an elementary coupled translational-rotational model of a rigid body as a basis for discussing the relative importance of various factors.

To investigate the coupling between translation and rotation of a rigid body under the influence of an external force acting at a point on the body away from the CM, consider the simplified two-dimensional problem illustrated in Figure A1. (For now, we ignore complications such as added mass, added moment of inertia, buoyancy, horizontal restoring forces, and damping.) The horizontal driving displacement x_0 is transferred to the body at a point a distance a below the CM. Rotation of the body is countered by a spring of angular spring constant k. The resulting motion is a combination of displacement (x) of the center of mass and rotation (θ) of the body about the CM. The body has mass m and moment of inertia I. For small angles the coupled equations of motion for x and θ are

$$F = m\ddot{x}, \tag{A1}$$

(force equals mass times translation acceleration),

$$Fa - k\theta = I\ddot{\theta}, \tag{A2}$$

(torque equals moment of inertia times angular acceleration),

$$x = x_0 - a\theta, \tag{A3}$$

(kinematic constraint), in which F (to be determined) is the force required to drive the body. Eliminating F between (A1) and (A2) and substituting (A3), the small-amplitude solutions are

$$\frac{x}{x_0} = 1 - \left(\frac{\beta}{1+\beta}\right)\frac{\omega^2}{\omega^2 - \omega_0^2}, \tag{A4}$$

$$\frac{a\theta}{x_0} = \left(\frac{\beta}{1+\beta}\right)\frac{\omega^2}{\omega^2 - \omega_0^2}, \tag{A5}$$

in which

$$\beta = ma^2/I \tag{A6a}$$

is an important dimensionless translation/rotation coupling parameter, and

$$\omega_0 = \sqrt{k/I(1+\beta)} \tag{A6b}$$

is the rocking resonance frequency.

As shown by DS, a horizontal velocity sensor rigidly mounted within the body a distance b above the CM senses

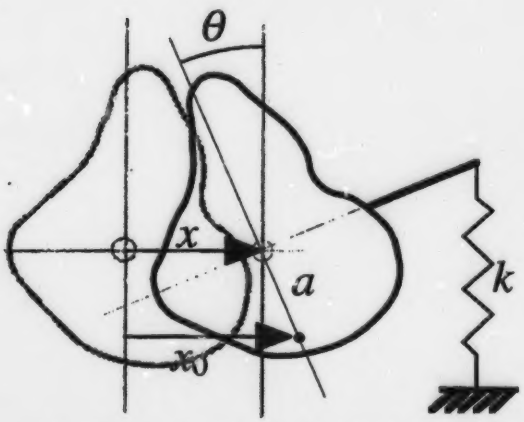

Figure A1. Translation and rotation of a rigid body pushed off center.

three components of motion: a translation of the CM (x), a rotation-induced translation ($-b\theta$), and a gravity-induced displacement directly linked to tilt ($g\theta/\omega^2$). The transfer function from driving displacement to sensor response is thus

$$T = \frac{x - b\theta + g\theta/\omega^2}{x_0}$$

$$= 1 + \left(1 + \frac{b}{a} - \frac{g}{a\omega^2}\right)\left(\frac{\beta}{1+\beta}\right)\frac{\omega^2}{\omega_0^2 - \omega^2}. \qquad \text{(A7)}$$

In the low-frequency limit the frequency-dependent factor in the gravity term cancels the frequency dependence of the resonance factor, giving

$$T \approx 1 - \frac{g}{a\omega_0^2}\left(\frac{\beta}{1+\beta}\right) \qquad (\omega \ll \omega_0). \qquad \text{(A8a)}$$

In the high-frequency limit,

$$T \approx 1 - \left(1 + \frac{b}{a}\right)\left(\frac{\beta}{1+\beta}\right) \qquad (\omega \gg \omega_0). \qquad \text{(A8b)}$$

At resonance, (A7) blows up, as we have not included damping, which we can readily add by making the substitution $\omega_0^2 \rightarrow \omega_0^2 + i\omega_0\omega/Q$, where Q is the quality factor of the resonance. With damping, at resonance the transfer function has the finite value

$$T = 1 - iQ\left(1 + \frac{b}{a} - \frac{g}{a\omega_0^2}\right)\left(\frac{\beta}{1+\beta}\right) \qquad \omega = \omega_0. \qquad \text{(A8c)}$$

Inspecting (A8a)–(A8c), we see that several conditions must hold for rocking to have negligible effect on the horizontal transfer function. First (and most importantly), the β factor must be small, that is, I must be large compared to ma^2. Second, the dimensionless gravity factor $g/a\omega_0^2$ must be small. If the rocking resonance frequency is well above the frequency range of interest, these conditions should suffice. However, if the rocking resonance is within the frequency range of interest, the above conditions must hold plus the ratio b/a must be of the order 1 or less and Q must be small, that is, the rocking resonance must be well-damped. In the context of OBS design, we are looking for an instrument having a large moment of inertia, a low CM, sensors below the center of mass, and a well-damped rocking resonance, preferably above the operating frequency range. Let us examine these requirements in turn.

A1. The β Factor

In OBS dynamics we must consider the role of added mass and added moment of inertia (AMOI) as well as the intrinsic mass and moment of inertia of the instrument. Attaching a large-diameter horizontal circular base plate to a spherical OBS vessel provides significant added mass for vertical motion (which is beneficial as we argue in section 2.2.4), without significantly increasing the added mass for horizontal motion (which would be detrimental). Moreover, the disk-entrained water and sediment provide significant added moment of inertia to the instrument.

In using (A6a) to estimate the translation/rotation coupling parameter β for the horizontal motion of an OBS consisting of a spherical vessel mounted on a circular base plate, the mass factor must be the sum of the inertial mass of the sphere, the mass of the disk, and the horizontal added mass of the sphere; the moment of inertia factor must include the moment of inertia of the sphere, the moment of inertia of the disk, and the disk AMOI. It is difficult to precisely define the AMOI for a disk on the seabed, as the flow of water is altered by the sediment boundary, and the OBS/sediment interaction itself probably contributes a sediment AMOI term. Also, if the CM height is an appreciable fraction of the base radius, the instrument will not rock about the plate axis, thus reducing the AMOI. However, for the purpose of supporting our assumption, which does not require a precise value, we argue that a reasonable order-of-magnitude estimate is provided by the AMOI formula for a circular plate in unbounded water. (This formula may be in doubt in case of combined translational/rotational motion.)

In the case of a horizontal force applied in the plane of the base, the moment arm is simply the height of the center of mass above the disk, which is 0.15 m for the ONR OBS and estimated to be 0.09 m for the DREA OBS. Using the numerical quantities from Table 1 for the DREA and ONR systems in (A6a), we estimate that $\beta_{DREA} \sim 0.11$ and $\beta_{ONR} \sim 1.3$. (For this calculation, m is the inertial mass plus the horizontal added mass, and I is the intrinsic moment of inertia plus the AMOI.) Because of the tentative nature of the formula used to calculate AMOI, these should be viewed as upper bound estimates; however, this exercise suggests that the two designs are an order of magnitude apart in their sensitivity to rocking effects. Regardless of the precise value of AMOI in these circumstances, it is safe to say that AMOI would scale as the fifth power of disk radius, so substantial reduction in rocking effects could be expected from a modest increase in coupling disk radius. At the same time, however, the horizontal added mass of sediment would increase a little, which would lower the horizontal resonance frequency, thus reducing the usable bandwidth.

A2. The $g/a\omega_0^2$ Factor

The parameter g is about 10 m/s^2 and a is of the order 0.1 m for a typical OBS. Using the Mathematica® notebook provided by DS, typical calculated rocking resonances appear to be in the range 11–32 Hz for the ONR and DREA OBSs, even on soft sediments. (This is deduced by "turning off" the rotational damping and noting the frequency of the sharp feature that appears in the transfer function.) Consequently, the low-

frequency dimensionless gravity factor $g/a\omega_0^2$ in (A8a) and (A8c) is of the order 10^{-2} or less. Moreover, even if one increases the value of g tenfold in the notebook calculations, the transfer function changes less than a decibel. The influence of this factor is clearly negligible for typical OBS designs.

A3. The b/a Factor

This is of the order 1 or less for most OBS designs (including the DREA OBS), and it would actually be better if it were negative rather than positive. (That is, put your sensor on the same side of the CM as the main driving force.)

A4. The Q Factor

As suggested above, the rocking resonances computed for both ONR and DREA OBSs are heavily damped, as it is necessary to numerically "turn off" the damping in order to actually see the resonances. This implies that Q is of the order 1 or less for rocking resonances of typical OBS designs. A low Q spreads the effect over a greater frequency range around the resonance, so this consequence must be carefully considered in combination with the other factors.

A5. Rocking in Response to a Shaker

The conclusions of the simple argument above still hold if one transfers the motion to the body through a compliant member. However, if one simultaneously forces the body at one point and attaches a restoring compliance at another point (as we do in an OBS calibration run), the problem becomes more complex. Leaving out the mathematical details, the effect is that the response of the sensor becomes modified at very low frequencies, as illustrated by Figure 6 of DS. Accordingly, one must be mindful of this potential contamination of the calibration data. The effect is substantially reduced by taking the measures already discussed: increasing the AMOI and keeping the CM low. Moreover, this effect is only an artifact of the calibration procedure, and its appearance in the low-frequency coupling data does not imply that the transfer function in response to seabed motion is affected.

A6. Added Moment of Inertia in the Model of *Dunnebier and Sutton* [1995]

DS have considered effects of rotational motion and tilt in their equations of motion for OBS dynamics and the expressions for sensor response. However, their model of OBS/seabed interaction is based on structure/soil models for a plate on an elastic half-space (with no water above). Accordingly, hydrodynamic inertial effects, both translational and rotational, of the water surrounding the OBS have not been accounted for in their expressions for the spring and damping coefficients. DS have explicitly corrected for this in the translation equations by adding estimates of the hydrodynamic added masses of the OBS in vertical and horizontal motion to the intrinsic mass of the instrument. However, in the rotational equations, they have not explicitly included the analogous rotational inertia of the water surrounding the instrument, i.e., the added moment of inertia (AMOI). If this was considered, it is an unstated assumption of their model that the fluid AMOI is negligible. This assumption may be justified in this case of the ONR OBS, which has a relatively narrow base plate and a high CM relative to the plate. On the other hand, for instruments with a wide bases and low CMs, such as the DREA OBS, the DS model would overestimate rocking effects through the neglect of the fluid AMOI term.

With respect to the inertial effects contributed by interaction of the base with the elastic sediment, the DS spring and damping coefficients probably already include them. We have argued in section 2.3 that a substantial part of the frequency dependence of the DS translational spring coefficients can be attributed to added-mass effects; it follows that the DS rotational spring coefficient also (in effect) includes sediment AMOI.

A7. Summary Comments

Consideration of the dynamics of an ideal rocking body provides several conditions that must be met for rocking effects to be considered negligible in the modeling of the transfer function for horizontal forcing in the frequency range of interest. We have argued, at least for the DREA OBS, that all conditions are met, and we are justified in ignoring rocking effects in our analysis. This assumption (and the associated theory) should hold for similarly designed instruments. Equipping an OBS with a large base plate to increase added moment of inertia to counter rocking motion appears to be a successful strategy that OBS builders may want to consider. If the DS model is used to simulate rocking motions of an OBS, the user is cautioned that there is a hidden assumption that the added moment of inertia of the water surrounding the instrument is negligible.

Acknowledgments. We would like to thank the officers and crew of Canadian Forces Auxiliary Vessel *Quest* for their assistance in the sea trials. LASMO Nova Scotia Limited kindly provided the daily reports on drilling operations of the Rowan Gorilla III at the Cohasset field. J. Osler was supported by a Visiting Fellowship at the Defence Research Establishment Atlantic and by the Canadian Acoustical Association through the Edgar and Millicent Shaw Postdoctoral Prize in Acoustics. We are indebted to George Watt of DREA for his hydrodynamic advice. Thanks also to Jack Dodds of GeoAcoustics, Inc. (Box 790, Aurora, Ontario, Canada L4G 4J9, (905)-727-8207). The authors thank all the reviewers for their constructive and challenging comments; these have resulted in a paper that more effectively communicates our message.

References

Batchelor, G. K., *An Introduction to Fluid Dynamics*, Cambridge Univ. Press, New York, 1967.

Bibee, D. E., and L. M. Dorman, Full waveform inversion of seismic interface wave data, in *Full Field Inversion Methods in Ocean and Seismo-acoustics*, edited by O. Diachok et al., pp. 377–382, Kluwer Acad., Norwell, Mass., 1995.

Canadian Seabed Research, Ltd., Seabed mapping for DREA experimental sites, DREA contractor report CR/96/404, 74 pp., Def. Res. Estab. Atl., Dartmouth, Nova Scotia, 1996.

Chung, H., and S. S. Chen, Hydrodynamic mass, in *Topics in Fluid Structure Interaction*, edited by H. Chung and M. D. Bernstein, p. 14, Am. Soc. of Mech. Eng., New York, 1984.

Courtney, R. C., and L. M. Mayer, Acoustic properties of fine-grained sediments from Emerald Basin: Toward an inversion for physical properties using the Biot-Stoll model, *J. Acoust. Soc. Am.*, *93*, 3193–3200, 1993.

Dodds, D. J., Seabed sound speed data analysis, DREA contractor report CR/90/404, 42 pp., Def. Res. Estab. Atl., Dartmouth, Nova Scotia, 1990.

Dodds, D. J., Acoustic sensor module for deployment on the seabed, DREA contractor report CR/94/459, 49 pp., Def. Res. Estab. Atl., Dartmouth, Nova Scotia, 1994.

Dodds, D. J., DREA ocean bottom seismometer improvements, DREA contractor report CR/95/498, 28 pp., Def. Res. Estab. Atl., Dartmouth, Nova Scotia, 1995.

Dodds, D. J., D. M. F. Chapman, J. C. Osler, and W. C. Risley, Minimizing instrument effects in an ocean bottom seismometer, *Can. Acoust.*, *22*, 161–162, 1994.

Duennebier, F. K., and G. H. Sutton, Fidelity of ocean bottom seismic observations, *Mar. Geophys. Res.*, *17*, 535–555, 1995.

Gregory, D. N., and P. C. Smith, Current statistics of the Scotian shelf and slope, *Can. Tech. Rep. Hydrogr. Ocean Sci.*, *109*, 38 pp., 1988.

Hedlin, M. A., and J. A. Orcutt, A comparative study of island, seafloor, and subseafloor ambient noise levels, *Bull. Seismol. Soc. Am.*, *79*, 172–179, 1989.

Kibblewhite, A. C., and K. C. Ewans, Wave-wave interactions, microseisms, and infrasonic ambient noise in the ocean, *J. Acoust. Soc. Am.*, *78*, 981–994, 1985.

Lamb, H., *Hydrodynamics*, 6th ed., p. 164, Dover, Mineola, N. Y., 1945.

Latham, G. V., and A. A. Nowroozi, Waves, weather, and ocean bottom microseisms, *J. Geophys. Res.*, *73*, 3945–3956, 1968.

Lewis, B. T. R., and J. McClain, Converted shear waves as seen by ocean bottom seismometers and surface buoys, *Bull. Seismol. Soc. Am.*, *67*, 1291–1302, 1977.

Louden, K. E., The collection and analysis of seismo-acoustic data: Results from Dalhousie ocean bottom seismograph recordings during CFAV *Quest* cruise Q211, DREA contractor report CR/94/416, 46 pp., Def. Res. Estab. Atl., Dartmouth, Nova Scotia, 1994.

Moran, K., R. C. Courtney, L. A. Mayer, A. A. Miller, and J. Zevenhuizen, Surficial geology and physical properties 12: Central shelf: Emerald Basin, in *East Coast Basin Atlas Series: Scotian Shelf*, p. 133, Geol. Surv. of Can., 1991.

Osler, J. C., A geo-acoustic and oceanographic description of several shallow water experimental sites on the Scotian Shelf, *DREA Tech. Memo. 94/216*, 47 pp., Def. Res. Estab. Atl., Dartmouth, Nova Scotia, 1994.

Osler, J. C., and D. M. F. Chapman, Seismo-acoustic determination of the shear-wave speed of surficial clay and silt sediments on the Scotian Shelf, *Can. Acoust.*, *24*, 9–20, 1996.

Sauter, A. W., Studies of the upper oceanic floor using ocean bottom seismometers, Ph.D. dissertation, Univ. of Calif., San Diego, 1987.

Stephen, R. A., et al., The seafloor borehole array seismic system (SEABASS) and VLF ambient noise, *Mar. Geophys. Res.*, *16*, 243–286, 1994.

Sutton, G. H., and F. K. Duennebier, Optimum design of ocean bottom seismometers, *Mar. Geophys. Res.*, *9*, 47–65, 1987.

Sutton, G. H., F. K. Duennebier, B. Iwatake, and J. D. Tuthill, An overview and general results of the Lopez Island OBS experiment, *Mar. Geophys. Res.*, *5*, 3–34, 1981a.

Sutton, G. H., F. K. Duennebier, and B. Iwatake, Coupling of an ocean bottom seismometer to soft bottom, *Mar. Geophys. Res.*, *5*, 35–51, 1981b.

Trehu, A. M., Coupling of ocean bottom seismometers to sediment: Results of tests with the U.S. Geological Survey ocean bottom seismometer, *Bull. Seismol. Soc. Am.*, *75*, 271–289, 1985.

Trehu, A. M., and G. H. Sutton, A note on the seafloor coupling characteristics of the new ONR ocean-bottom seismometer, *Mar. Geophys. Res.*, *16*, 91–103, 1994.

Watkins, W. A., P. Tyack, K. E. Moore, and J. E. Bird, The 20 Hz signals of finback whales (*Balaenoptera physalus*). *J. Acoust. Soc. Am.*, *82*, 1901–1912, 1987.

Wolfram, S. *Mathematica: A System for Doing Mathematics by Computer*, 2nd ed., 961 pp., Addison-Wesley, Reading, Mass., 1991.

Zelikovitz, S. J., and W. A. Prothero Jr., The vertical response of an ocean bottom seismometer: Analysis of the Lopez Island vertical transient tests, *Mar. Geophys. Res.*, *5*, 53–67, 1981.

D. M. F. Chapman, Defence Research Establishment Atlantic, P.O. Box 1012, Dartmouth, Nova Scotia, Canada B2Y 3Z7. (e-mail: chapman@drea.dnd.ca)

J. C. Osler, SACLANT Undersea Research Centre, Viale San Bartolomeo 400, 19138 La Spezia, Italy. (e-mail: osler@saclantc.nato.int)

(Received February 11, 1997; revised December 22, 1997; accepted January 27, 1998.)

#509233